Relating Laboratory and Outdoor Exposure of Coatings: II.

Effects of Relative Humidity on Photodegradation and the Apparent Quantum Yield of Acrylic-Melamine Coatings

Tinh Nguyen, Jonathan Martin, Eric Byrd, and Ned Embree—
National Institute of Standards and Technology*

The effect of relative humidity (RH) from <<1% to 90% on the photodegradation and quantum efficiency for a partially-methylated melamine acrylic coating exposed to UV/50°C condition has been investigated. The UV source is supplied by two 1000 W Xenon arc solar simulators and the relative humidities are provided by specially designed humidity generators, which control relative humidity in the 0 to 90% range to within < 3% of the measured values. Radiation absorbed in the coating and degradation of the films are measured by UV-visible and Fourier transform infrared spectroscopies, respectively. The degradation at a particular RH/UV condition consists of four different modes: reactions taken place during post curing, hydrolysis due to water in the film at a particular RH, photodegradation, and moisture-enhanced photodegradation. Total degradation, hydrolysis, and moisture-enhanced photodegradation increase with increasing RH. At low relative humidities, photodegradation is an important degradation mode but hydrolysis dominates the degradation at high RH levels. Moisture in the film is found to increase the quantum efficiency of acrylic melamine coating photodegradation.

INTRODUCTION

Weather patterns are never duplicated.[1] This deficiency may explain the lack of progress in relating short-term performance with outdoor test and in predicting accurately the service life of polymeric materials. This investigation is part of a comprehensive study to generate experimental data for validating the total effective dosage model[2] for predicting the service life of organic coatings. The total effective dosage concept, which has been applied successfully in medical and biological fields,[3,4] is based on the principles of photochemistry.[5] The use of total effective dosage, instead of total solar irradiance or total elapsed time as traditionally employed,[6-8] takes into account the fact that not all ultraviolet (UV) radiation is absorbed and not all absorbed radiation photolytically degrades a material.

The effective dosage is related to damage through the spectral quantum yield. The latter is the photolytic damage incurred per unit of incident radiation at each wavelength or within a range of wavelengths.[9] For the photodegradation of polymeric materials, quantum yields depend not only on the physical and chemical properties of the material but also on environmental factors, such as moisture and temperature.[10-13] It is, therefore, essential to design short-term tests to provide effective dosages and quantum yields over wide ranges of temperature and humidity so as to cover a wide range of conditions to which a polymeric coating is expected to be exposed in the field and to permit the deconvolution of the effects of these factors on the degradation.

In a previous publication, we described in detail the methodology used to determine the absorbed dosage in the coatings, the apparent quantum yield over a wide range of exposure conditions, and the factors critical to the accuracy and reproducibility of these quantities.[14] UV-visible and Fourier transform infrared (FTIR) spectroscopies were used to measure the absorbed dosage and quantum yield. Both the absorbed dosage and apparent quantum yield were found to be extremely sensitive to a number of variables, including the initial UV-visible absorption of the coatings, coating degradation products, data processing of infrared and UV-visible spectra, and the reproducibility of UV-visible and FTIR spectrometers.

This paper presents the results of the effects of relative humidity (RH) on the degradation and quantum yield of a

*100 Bureau Dr., Stop 8621, Gaithersburg, MD 20899.

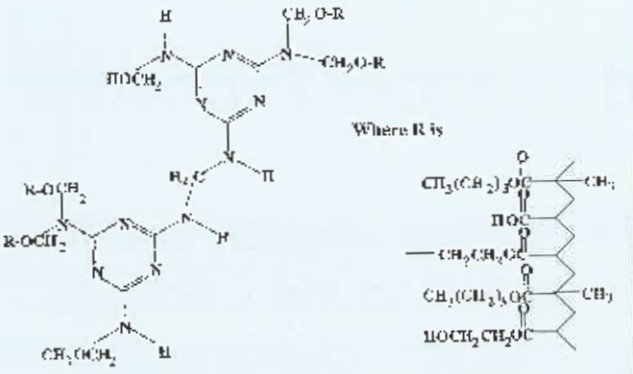

Figure 1—Postulated chemical structure of the partially-methylated melamine acrylic coating used in this study.

model partially-methylated melamine acrylic coating exposed to UV-visible radiation. This coating was selected because of its extensive use in automotive clearcoat/basecoat systems. The influence of RH on the hydrolysis rate and a postulated mechanism of hydrolysis in the absence of light are also presented. Although a combination of five RH levels ranging from <<1 to >90% under four different temperatures and 12 different UV spectral conditions were investigated, only the results of relative humidities at 50°C in the presence and absence of UV light are reported here. It should be noted that, although coated panels exposed to the outdoors may never experience the 50°C and 90% RH at the same time, the high humidity was included in this study to better understand the magnitude of relative humidity effect on the degradation of this coating. The effects of UV wavelength and temperature on the quantum yield and photodegradation will be addressed in future publications.

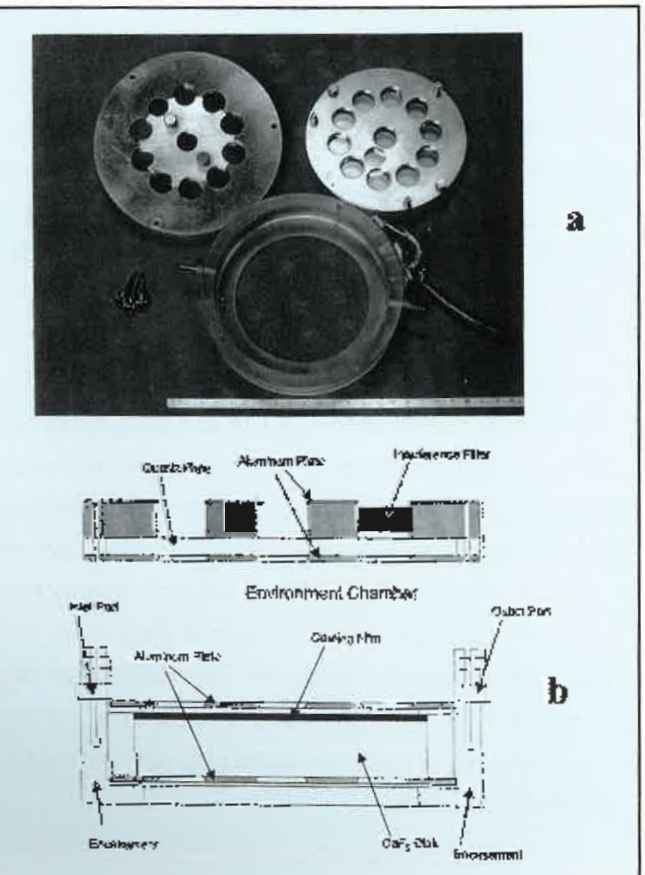

Figure2 —(a) A photograph showing an exposure cell and (b) cross section showing the quartz plate, the coated CaF_2, and the space containing the exposure environment.

Photodegradation of acrylic-melamine coatings in the presence and absence of UV stabilizers has been extensively studied.[15,16] In the absence of moisture, photoinduced chain scission in acrylic melamine coatings is a free radical-initiated oxidation process,[16] with the formation of amines and various carbonyl derivatives as the degradation products.[17] Ketonic end groups present in the acrylic resin have been identified as the main chromophores responsible for initiating the photooxidation reactions of these coatings.[18,19] A secondary pathway involved in the formation of urethane groups has been suggested for the UV irradiation of melamine clearcoats, and these urethane groups are believed to contribute to the improved etching resistance of conventional acrylic-melamine coatings.[20]

The photodegradation chemistry of acrylic melamine coatings in the presence of moisture is more complex. The most intensive study on the subject was conducted by Bauer and co-workers,[21,22] in which relative humidities were varied by changing the dew point temperature. In the early study,[21] the exposure temperature was maintained at 60°C and dew point temperatures were controlled at 50°, 25°, and –40°C. From the Table of Vapor Pressure of Water,[23] these air temperature/dew point temperature pairs correspond to 62% RH, 16% RH, and 0.06% RH, respectively. In the later study,[22] the air temperature was 40°C and the dew points were set at 25°C (42.8% RH) and –10°C (3.5% RH). Obviously, these levels do not cover the range of relative humidity that can be encountered during outdoor exposure. In both studies, the rate of hydrolysis in the presence of UV light was found to be greater than the sum of dark hydrolysis and photodegradation combined. The acceleration was attributed to melamine excited-state chemistry. Gerlock et al.[24,25] also reported accelerated hydrolysis under UV conditions, and postulated that the formaldehyde released from the photodegradation reactions may be involved in the enhancement. On the other hand, English and Spinelli[26,27] suggested that the greater degradation of fully-alkylated acrylic melamine coatings exposed in Miami, FL, compared with one exposed in Phoenix, AZ, is due to the carboxylic acids formed during photooxidation of the coating. Using well-controlled, dry air/moisture-saturated air mixture relative humidity generators, Nguyen, Martin, and co-workers[28] have recently quantified the effects of relative humidities ranging from <<1 to >90% on the moisture-enhanced photodegradation of partially-methylated melamine acrylic coatings. They found that the enhancement of both the acrylic-melamine crosslink scission and the acrylic side chain cleavage increased with increasing RH. Further, the enhancement followed closely with changes in the hydrolysis rate.

Because acrylic melamine coatings are known to be susceptible to etching during outdoor exposure, the degradation characteristics of these materials exposed to water, high humidity, and acid-rain environments in the absence

and presence of UV light have been investigated.[29-34] For example, it has been observed that during dark hydrolysis, which is much greater for partially-alkylated melamine than for fully-alkylated melamine-based coatings, the acrylic-melamine crosslinks are broken and melamine-melamine linkages are formed.[29] Further, the rate of hydrolysis depends on the type of acid curing agent, the temperature, and the melamine resin chemical structure. In mild organic acids, the acrylic-melamine crosslinks were found to hydrolyze faster than the unreacted methoxy groups of the melamine.[29] However, in strong inorganic acid solutions, the melamine methoxy was observed to hydrolyze first, followed by the hydrolysis of the crosslinks.[30] Partially-alkylated melamine acrylic coatings undergo etching in sulfuric acid environments first by permeation of the acid into the film, which promotes hydrolysis of the crosslinks to form melamine derivatives, followed by an extraction of melamine derivatives by the acid.[31] Extensive results of outdoor exposures and accelerated tests containing acid rain elements have indicated that the degradation of acrylic melamine coatings is strongly influenced by UV, RH, and air pollutants.[32-34]

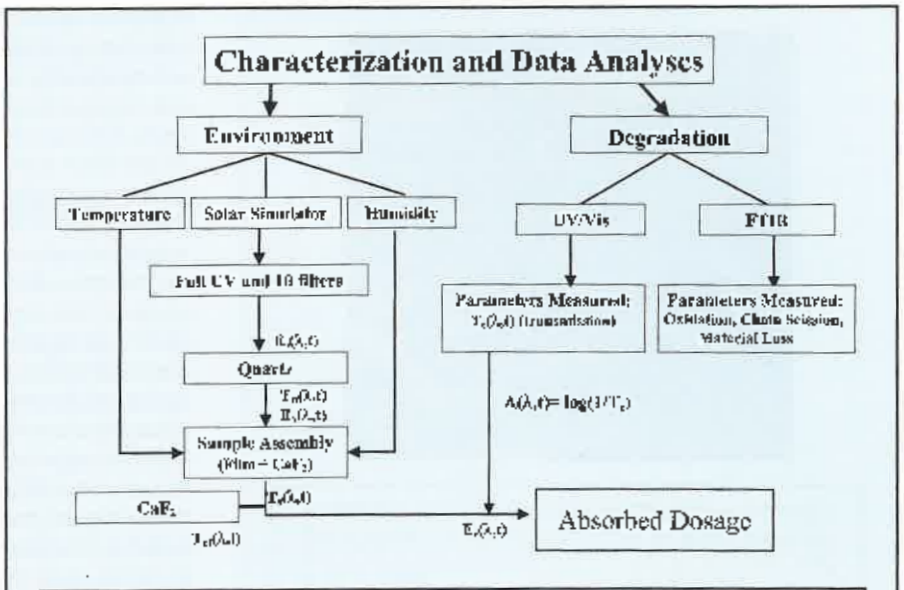

Figure 3—Flowchart displaying the various stages for measuring coating damage and absorbed dosage in the presence of UV, relative humidity, and temperature.

EXPERIMENTAL CONDITIONS AND PROCEDURES*

Materials and Specimen Preparation

A model acrylic melamine coating was selected for the current study because this type of polymer has been used in a variety of applications.[35] The coating films were prepared from a mixture of a hydroxy terminated acrylic resin and a partially-methylated melamine resin. The acrylic material contained 68% normal butylmethacrylate, 30% hydroxyethylacrylate, and 2% acrylic acid. It was supplied as a mixture of 70.2% acrylic polymer and 29.8% 2-heptanone as a solvent. The melamine resin was Cymel 325* (Cytec Industries), which is a mixture containing 69.0% partially-methylated melamine resin and 31% isobutanol solvent. The ratio of acrylic resin to melamine resin was 70:30. All percentages and proportions are expressed as mass fraction. It should be noted that this model acrylic-melamine coating contained no strong acid catalyst and no light-stabilized additive (e.g., hindered amine and UV absorber). Calcium fluoride (CaF_2) plates with a diameter of 100 mm and a thickness of 2 mm were selected as the substrate for the exposure study due to their transparency in the 0.13 to 11.5 μm wavelengths and their resistance to moisture and heat.[36] Therefore, it was possible to independently expose clear coatings applied to CaF_2 substrate to wide ranges of temperature, humidity, and UV radiation, while monitoring the spectral absorption of the coating by UV-visible spectroscopy and coating degradation by FTIR transmission spectroscopy.

Coatings were applied to CaF_2 plates by spin casting. Acrylic and melamine resins in solvents were mixed at the required ratio, degassed, flooded onto the substrates, and spun at 2000 rpm for 30 sec. The coatings were then cured at 130°C for 20 min. All coated samples were well cured, and coating thickness was uniform within approximately 97% for the entire coated surface, as shown by FTIR analysis on different locations of the coated CaF_2 plates after curing. Based on FTIR evidence, the cured coating material used in this study had a chemical structure close to that shown in *Figure* 1.

Instrumentation and Exposure Cells

Complete details on the exposure cell, UV light source (i.e., solar simulator), instrumentation, and controlled systems are given in reference 14. This section briefly describes some instruments and experimental procedures that are pertinent to this study. The UV light source consisted of two 1000 W Xenon arc solar simulators. Each simulator was equipped with a dichroic mirror to remove the majority of the infrared and visible radiation and a photofeedback controller to regulate the light intensity. Thus, the temperature of the area irradiated by these solar simulators was at most 2°C above ambient (24°C) temperature. The radiation from the simulators covers the wavelength range from 275 to 800 nm. The relative humidities were provided by custom-designed humidity generators, which were fabricated on the principle of proportionally mixing dry air and moisture-saturated air. Each individual humidity generator is capable of supplying up to four different levels of RH. The relative humidities could be independently controlled

*Certain commercial products or equipment are described in this paper in order to specify adequately the experimental procedure. In no case does such identification imply recommendation or endorsement by the National Institute of Standards and Technology, nor does it imply that it is necessarily the best available for the purpose.

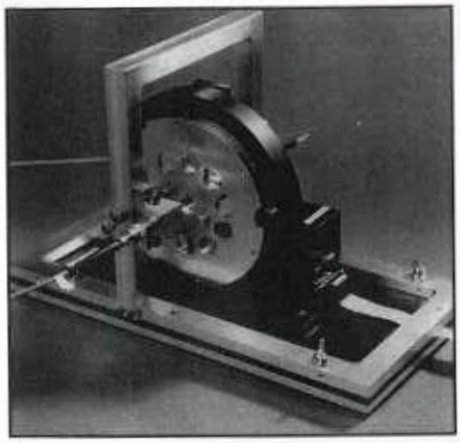

Figure 4—A photograph showing the autosampling accessory with the exposure cell placed in it.

and maintained to within approximately 3% of their preset values for RH from 0 to 90%. The temperature within each humidity generator was controlled within ±1°C in the range from 30° to 60°C by the use of temperature feedback control devices, heating coils, and thermocouples.

The exposure cells were designed to simultaneously expose different sections of the same film to different combinations of temperature, RH, and UV radiation. *Figure* 2a is a photograph of one exposure cell (together with the interference filter holder and the cell holder), and *Figure* 2b schematically illustrates the cross-section of the exposure cell. Each cell consisted of a 12-window aluminum frame and a 100 mm diameter CaF_2 plate with an approximately 10 μm thick acrylic melamine film applied to it. Ten of the windows contained interference filters (each filter transmitting a particular wavelength range of interest); one window was completely covered with an aluminum plate to prevent radiation from reaching the coating (designated as no-UV or dark specimen), and one, located in the center of the cell face, was left open without any filter. The coating area within the open window is designated as the "full UV" specimen because it received the unfiltered radiation of the solar simulator. Each window enclosed a 19 mm diameter hole through the aluminum plate with a bevel to support an interference filter. Care was taken to ensure that no radiation strayed onto the no-UV (covered) coating area. All windows were constructed with knife edges to prevent grazing angle reflections from the sides of the windows. The quartz plate was placed directly underneath the aluminum frame and 9 mm above the coated CaF_2 plate to protect the filters from the exposure environments. Each exposure cell contained an inlet and an outlet that allowed fresh air of the desired temperature and RH to continuously enter the sample exposure chamber and let the outgoing air vent to the outside of the chamber. Each exposure cell was equipped with a thermocouple and a chilled-mirror hygrometer to monitor temperature and relative humidity, respectively.

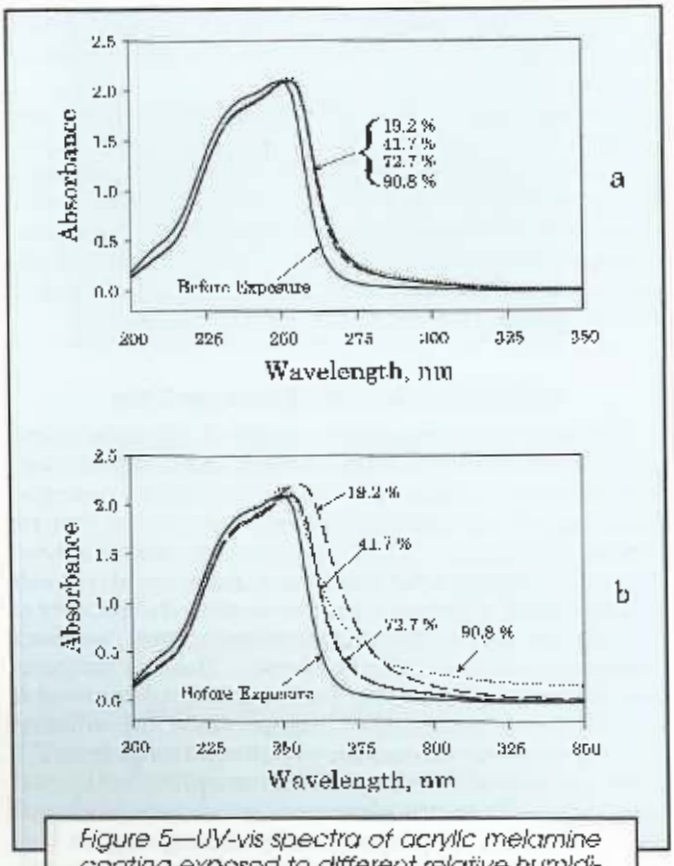

Figure 5—UV-vis spectra of acrylic melamine coating exposed to different relative humidities for 1536 hr in the absence (a) and presence (b) of "full UV" light.

Characterization of Exposure Environments

Specimens were exposed to different combinations of temperature, RH and UV-visible radiation. Nominal RH levels of 0, 20, 40, 70 and 90% at nominal temperatures of 30°, 40°, 50° and 60°C, and 12 different UV conditions consisting of no UV, "full UV," and 10 different wavelength regions were employed. *Figure* 3 presents a schematic diagram depicting various measurement stages of the environment (temperature, RH, and UV light intensity and spectral distribution) affecting the samples. The RH at a specified temperature in each cell was tracked by a feedback-control system, which monitored both the temperature and RH within the exposure cell three times per second.

A UV-visible spectrometer connected to a robotic controlling system by a fiber optic cable was used to record the UV-visible spectrum for each specimen at each of the 12 windows. The robotic-controlled fiber optic cable probe had the capability of moving in the X, Y, and Z directions, and the spectrometer was programmed to make these measurements at frequent time intervals. The measurements were made in the presence and absence of the exposure cells. Spectra taken in the absence of the cells recorded the UV lamp intensity at that particular location. Spectra in the presence of the cells recorded the transmission of light passed through the quartz plate and the coated CaF_2 plate. Transmission measurements were also taken individually for the quartz, the coated CaF_2, and the bare (uncoated) CaF_2 plates. These measurements allowed us to follow changes in lamp intensity and changes in transmittance of the quartz and CaF_2 plates during the exposure. From the amount of light transmitted through each compo-

nent of the exposure cell as a function of time, the light intensity impinging upon, as well as absorbed by, the coatings was determined. Both of these quantities are required inputs for estimating the absorbed dosage and quantum yield.

Measurement of Coating Degradation

UV-Visible Spectroscopy: UV-visible spectra of the coating and its changes during exposure were measured by UV-visible spectroscopy. This information was used for calculating the total dosage absorbed in the coatings as a function of exposure. At each specified time interval, the coated CaF_2-contained exposure cell was removed from the exposure cell and fitted into a demountable 150 mm diameter ring of a PIKE® autosampling accessory (*Figure* 4). The ring was computer-controlled and can be programmed to rotate and translate over the entire sampling area. Spring-loaded Delrin clips ensure that the specimens are precisely located and correctly registered. The autosampler was placed in the UV spectrometer compartment and UV-visible spectra were taken at 2 sec per scan using a customized computer program. This automated sampling system allowed unattended, efficient, and quick recording of the UV transmission of the coating at all 12 windows of an exposure cell. Since the exposure cell was mounted precisely on the autosampler, error due to variation of sampling at different exposure times was essentially eliminated. The radiation absorbed by the coating was obtained after subtracting the transmission of the uncoated CaF_2 plates from that of the coated CaF_2 plates.

Fourier Transform Infrared (FTIR) Spectroscopy: Damage in the coating was followed by transmission FTIR spectroscopy. FTIR techniques, both in the reflection and transmission modes, have been demonstrated as good analytical tools for quantifying the degradation of clear and pigmented coatings.[37,38] FTIR transmission spectra were taken using the same PIKE autosampler described above placed in an FTIR spectrometer equipped with a liquid nitrogen-cooled mercury cadmium telluride (MCT) detector. All FTIR spectra were the average of 132 scans recorded at a resolution of 4 cm^{-1} using dry air as the purge gas. The peak height method was used to represent IR intensity, which is expressed in absorbance, A. Except for the <<1% RH both in the presence and absence of UV at 50°C where the values of IR absorbance were the average of four specimens, the results for other relative humidities were from measurements of one specimen. Therefore, uncertainties are provided only for the <<1% RH results.

In addition to measurement of degradation, several other FTIR analyses of the coatings were also conducted to aid in the identification of IR bands in the coatings before and after degradation. These include in-situ monitoring of the coating curing process and deuterium oxide (D_2O) treatment of coated specimens that had been exposed to UV light with and without humidity. For the FTIR in-situ curing study, coatings approximately 1 ± 0.1 μm thick were cast on 25 mm diameter NaCl plates. An aluminum holder, typically used for IR transmission measurements, was wrapped with an electrical heating tape to provide a specimen heating enclosure. The heating tape was connected to a voltage-controlled device for regulating the temperature.

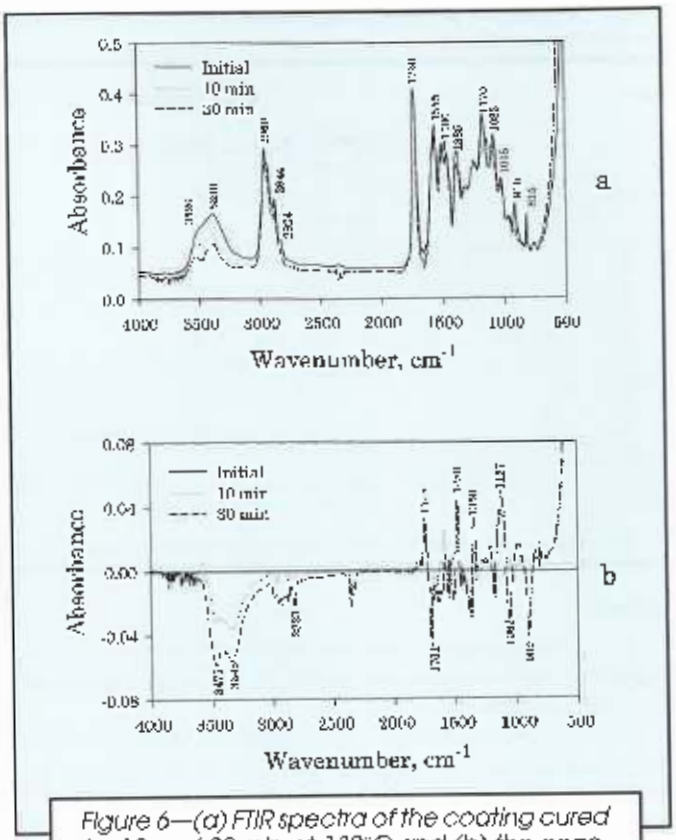

Figure 6—(a) FTIR spectra of the coating cured for 10 and 30 min at 130°C and (b) the corresponding FTIR difference spectra.

A thin thermocouple was placed between the coated specimen and the holder support to follow the temperature of the coatings during heating.

Deuterium oxide treatment of degraded specimens was performed on films cast on 3 mm thick, 25 mm diameter CaF_2 substrates. D_2O treatment effectively replaces the H atom of the OH and NH groups with a D atom. This substitution decreases the FTIR intensity of the OH and NH bands and, thus, facilitates the identification of the bands associated with these groups in the coatings. Coated films of approximately 2 μm thick that had been exposed to the "full UV," / 20 RH / 50°C condition for 600 hr were used. It has been observed that, under this condition, the coating degrades substantially and the FTIR intensity of all bands changes with exposure time. Specimens were positioned horizontally on a support in a sealed jar containing reagent grade D_2O in such a way that no liquid D_2O was in contact with the specimens. The sealed jar containing the specimens was placed in a 60°C oven, and FTIR spectra of the treated specimens were taken at specified intervals

Determination of Absorbed Dosage and Apparent Quantum Yield

Quantum yield is expressed as the damage that occurs per unit of incident radiation on a sample. Damage in polymers or coatings can be measured from various products formed during the photodegradation of polymers using a number of analytical techniques. In this study, quantum yield is estimated by:

$$\phi(\lambda) = D_{(dam)}(\lambda, t) / D_{abs}(\lambda, t)$$

Table 1—Selected IR Band Assignments for a Cured, Partially-Methylated Melamine Acrylic Coating Before and After Exposure To RH/UV Conditions

cm^{-1}	Band Assignment	Remark	Reference
3520	OH str. (acrylic resin)[a]	also reformed	
3470	OH str (methylol)	formed, moist environment	
3380	OH str. and NH str.		(47)
3330, 3230	NH str.	formed, moist and dry with/without UV	
2825	CH str. of OCH_3		(49)
1760	C=O str. of ?	formed, dry UV	
1705	C=O str., carboxylic acid	formed, moist/no-UV, dry or moist/UV	
1670	C=O str. of amide	formed, moist/no UV, dry or moist/UV	
1630	NH bending of NH_2	formed, moist/no-UV, dry or moist/UV	
1555	exo-CN + quad. – CH_2		(48)
1480	CNH of $-N-CH_2-N-$		
1350	$-N-CH_2-N-$		(47)
1170	C–O str. of the O–C=O group		
1085	C–O str.		
910	C–O str. of OCH_3 + sextant o.p. bend		(48)
815	sextant o-pl bending		(49)

(a) Abbreviations: str: stretching; semi-str: semi-circle stretching; o-pl: out-of-plane; quad.: quadrant; exo-CN: CN bond directly attached to the triazine ring.

where

$\phi(\lambda)$ = apparent quantum yield within the exposed radiation wavelengths, in $A m^{-1} J^{-1}$ (A is IR absorbance and m is film thickness),

$D_{abs}(\lambda,t)$ = absorbed dosage within the radiation wavelengths generated by the solar simulators at time t, in J,

D_{dam} = damage, in IR absorbance (A) units.

The procedure for measuring and calculating the absorbed dosage has been described in detail elsewhere.[14] The absorbed dosage was obtained by integrating the product of the spectral irradiance, $E_t(\lambda,t)$, and the spectral absorption of the coating, $(1-10^{-A(\lambda,t)})$, over the wavelengths of radiation impinging on the specimen for the exposure duration at a particular humidity and temperature. $E_t(\lambda,t)$ is the product of a set of lamp irradiance spectra and quartz plate transmission spectra, and $A(\lambda,t)$ is the UV-visible absorbance of the specimen taken from the UV-visible absorption spectrum. Both of these quantities were measured, as previously described.

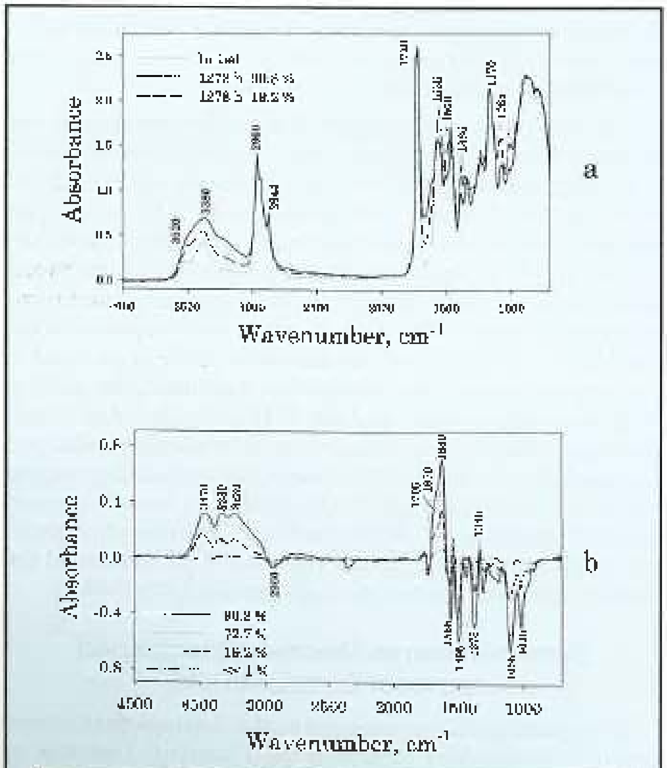

Figure 7—(a) FTIR spectra for specimens before and after exposure to 90.8% and 19.2% RH under no-UV at 50°C for 1278 hr and (b) FTIR difference spectra for four relative humidities under no UV/50°C condition for 1278 hr.

An apparent quantum yield can be estimated by taking the initial slope of the curve relating absorbed dosage and damage. For the acrylic melamine coatings, significant hydrolysis was observed even in specimens not exposed to the UV lamps. This dark hydrolysis effect must be removed before the FTIR degradation data can be used to estimate the absorbed dosage. This was accomplished by subtracting the spectra of the dark specimens from those of the irradiated specimens at the same temperature and RH. Damage is then expressed as the change of the IR absorbance of a functional group with time, or, for photolytically sensitive reactions, with absorbed dosage, i.e., the energy remaining in the specimen.

Damage was measured using FTIR spectroscopy. This technique monitors the loss or the formation of chemical functionalities as a function of exposure time or absorbed photolytic dosage. Thus, the quantum yield in this study is an "effective" or "apparent" quantum yield and is expressed as the change in FTIR intensity per unit thickness per amount of radiation absorbed in the coatings. Decker et al.[39,40] have also employed FTIR spectroscopy for estimating the quantum yields of a number of coatings irradiated by mercury and fluorescent lamps. If FTIR intensity of the degradation is expressed in absorbance units (A), thickness in meters (m), and radiation dosage absorbed by the coating is expressed in Joules (J), the apparent quantum yield is expressed in $A m^{-1} J^{-1}$.

RESULTS AND DISCUSSION

Stability and Uniformity of UV-Visible Light Source

Spatial uniformity and stability of the UV-visible light source as a function of exposure time have been presented

in reference 14. In general, the radiant intensity is spatially and temporally nonuniform. For example, the mean radiant energy difference between the two solar simulators is 310 W/m² (640 W/m² and 950 W/m²). Further, the coefficients of variation of the radiant flux over the surface area for each of the two simulators are high (16% and 22%). The light source is observed to age with time, and the rate of the aging is different for each wavelength. For example, after 1500 hr of continuous operation, the radiant energy losses (with respect to initial values) at 290, 326, and 450 nm are 25, 50, and 38%, respectively. There is no detectable change in the transmittance of the CaF_2 and a small transmittance loss in the quartz plates during the course of exposure. All of these changes are accounted for in the calculation of the radiation absorbed in the samples.

Control of Relative Humidity and Temperature

Both temperatures and relative humidities were well controlled. The coefficients of variation of the five RH levels studied, i.e., 0.002, 19.2, 40.7, 72.7 and 90.8% are within 3.0% of the measured values, and the standard deviation of temperature for the 50°C exposure is 0.5°C. The 0.002% RH is estimated from the Table of Vapor Pressure of Water,[23] given the 50°C exposure temperature and the −70°C dew point (temperature of the dried air before entering the 50°C heated mixing chamber). The RH measurement instrument, i.e., the chilled mirror hygrometer, is not sensitive enough to record this low RH. Hereafter, the 0.002% RH is designated as << 1% RH or dry. Relative humidities produced by the method of mixing dry air and moisture-saturated air are found stable during the course of exposure, even at elevated temperatures, and essentially eliminate the introduction of contaminants on sample surfaces.

UV-Visible Spectroscopic Analysis

Since the absorbed dosage and quantum yield depend strongly on the UV-visible absorption characteristics of the coatings, careful UV-visible analysis of the coatings before and during exposure is essential to provide credible data for model verification. *Figures* 5a and 5b display the UV-visible spectra of the cured acrylic-melamine coating before and after exposure for 1536 hr to different RH levels in the presence and absence of UV light, respectively. The thickness of these samples was 10 ± 1.2 μm. The cured coating absorbs strongly only at wavelengths below 265 nm, indicating that the UV-visible radiation produced by the solar simulators used in this study (from 275 to 800 nm) is mostly transmitted through the film. Absorption at wavelengths above 275 nm is very small. Costa et al.[41] have reported a weak absorption near 300 nm in the melamine molecules, and Bauer and Briggs[21] have suggested that this absorption probably contributed to the photoenhanced hydrolysis of acrylic-melamine coatings exposed to moisture in the presence of UV light.

In the absence of UV light, the presence of moisture causes a small shift to higher frequency in the 265 to 270 nm region and an increase in intensity in the 270 to 300 nm region. Both the shift and absorption increase are greater in the presence of UV (compare *Figure* 5a with *Figure* 5b). The reason for these changes is not known. However, as will be presented in the FTIR results, various carbonyl-containing compounds were formed during the photodegradation of

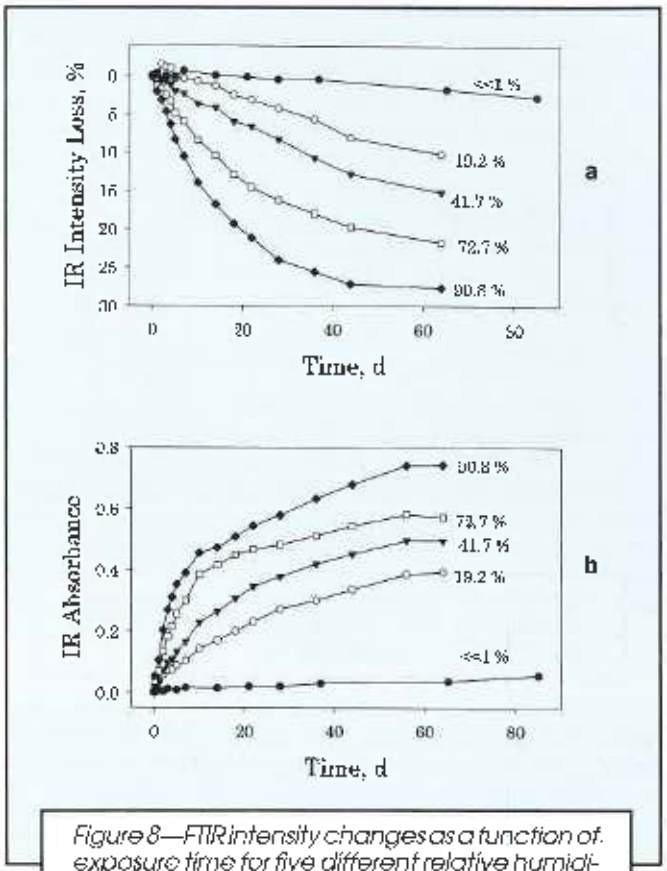

Figure 8—FTIR intensity changes as a function of exposure time for five different relative humidities at 50°C in the absence of UV: (a) 1085 cm⁻¹ band, and (b) 1630 cm⁻¹ band.

acrylic-melamine coating in the presence and absence of moisture. Additionally, Fox et al.[42] have observed an absorption increase in the region from 260 to 300 nm in the UV-vis spectra of poly(methyl acrylate) irradiated in air, and attributed this increase to the formation of formaldehyde in the polymer chains. Gerlock et al.[25] have also reported a substantial amount of formaldehyde generated during the photodegradation of acrylic melamine coatings and that three quarters of this formaldehyde remains in the films.

FTIR Analysis of Coating before Exposure

The performance and durability of polymeric coatings are mainly determined by the chemical structure of the cured film. For acrylic-melamine coatings, the cured structure is primarily controlled by the functionalities of the melamine resin.[43] As indicated in the experimental section, the melamine resin used in this study was a partially-methylated material, which is a complex mixture of different compounds with varying degrees of substitution.[44] In addition to the methoxymethyl functionality ($-CH_2OCH_3$), a partially-methylated melamine resin also contains substantial amounts of imino (–NH) and methylol ($-CH_2OH$) groups. There are many possible reactions that can take place during the curing of a partially-alkylated melamine resin with a hydroxy-terminated acrylic ester used in this study.[45,46] For example, in addition to the formation of the melamine-acrylic crosslinks between the melamine methoxy and the acrylic hydroxy, the residual methylol groups in the melamine can self-condense to form melamine-

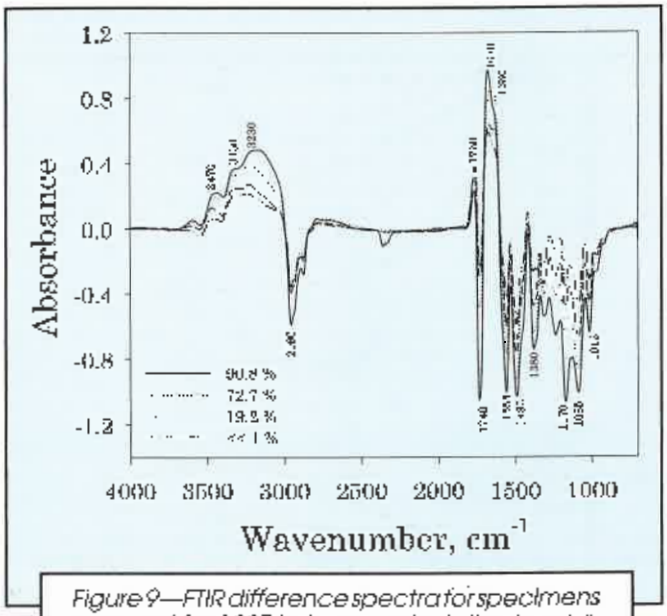

Figure 9—FTIR difference spectra for specimens exposed for 1287 hr in several relative humidities at 50°C in the presence of "full UV."

melamine linkages. Thus, the cured coatings contain a variety of groups and linkages that will affect the degradation of the coatings when exposed to the outdoors.

FTIR spectra of the coating before and after curing for two different times are presented in *Figure* 6a, and the corresponding difference spectra are shown *Figure* 6b. These spectra are obtained from an in-situ curing of a 1 μm film applied to an NaCl plate heated to 130°C. The major bands of interest in a cured film are the absorptions peaking at 3520 cm^{-1}, due to the OH group of the acrylic resin, near 3390 cm^{-1}, due to OH / NH groups of the melamine resin,[47] and at 1085 cm^{-1}, due to –C–O–C groups. Based on force field calculations and Raman and FTIR analyses, Larkin et al.[48] have recently assigned the band near 1555 cm^{-1} to contributions from three different groups: the triazine ring, CN attached to the ring, and CH_2. The other two important functionalities frequently used for curing and degradation analyses of melamine-based materials are the bands at 910 cm^{-1}, due to OCH_3 and semicircle stretch,[48] and at 815 cm^{-1}, due to the triazine ring out-of-plane deformation.[49]

Difference spectra of *Figure* 6b reveal that, during curing, the intensity of a number of bands decreases, including those in the 3600 to 2800 cm^{-1} region and near 1701, 1062, 1375, and 910 cm^{-1}. The intensity decrease of the 1701 cm^{-1} band (assigned to carboxylic acids C=O, together with the formation of the band at 1748 cm^{-1} (assigned to ester C=O) suggests that some esterification has occurred during curing. Several new bands appear after curing, including those at 1748, 1480, 1350, and 1127 cm^{-1}. The band at 1350 cm^{-1} has been assigned to the methylene bridge, –N–CH_2–N–,[47] which is formed by the self-condensation of the –N–CH_2OH groups of the melamine chains.

The band at 1480 cm^{-1} is assigned to the CNH bonds associated with the acyclic or cyclic –N–CH_2–N– bridges. This assignment is supported by FTIR spectral data obtained after further heating the 130°C-cured sample at 180°C for an additional 15 min. The spectra of the heated samples show that the intensities of the 1480 and 1350 cm^{-1} bands increase with the heat treatment. This increase corresponds with a decrease in intensity of the bands at 3375, 2825, 1085, and 910 cm^{-1}. Further, based on NMR evidence, Samaraweera and Jones[50] have shown that the singly-substituted –NH– (CH_2OCH_3) groups in the melamine chains self-condense readily to form an acyclic –N–CH_2–N– bridge and the doubly-substituted –N–(CH_2OCH_3)$_2$ groups are converted to a cyclic –NCH_2N– bridge after heating at 100°C. Since the 2825, 1085, and 910 cm^{-1} bands are associated with the $-CH_2OCH_3$ group, the heating experiment results suggest that the 1480 cm^{-1} band is associated with the CNH bonds in the NCH_2N– linkage. This assignment is also consistent with our observation that the intensity of this band decreases rapidly with exposure in humid environments. Both acyclic and cyclic –NCH_2N– bridges are unstable in the presence of water.

Additional FTIR analyses of acrylic and melamine resins before mixing, melamine model compounds, and literature support the assignments of pertinent bands given in Table 1. This table also includes the major bands formed during exposure in different environments.

Effects of Relative Humidity on Degradation in the Absence of UV

Figure 7a presents typical FTIR spectra before and after exposure for a specified time at 50°C under two different RH levels in the absence of UV light (no UV). The samples used for exposures are fully cured, as evidenced by the FTIR intensities of the bands at 910 cm^{-1} and 2825 cm^{-1} (associated with the OCH_3 group), which remain constant after the 20 min curing at 130°C. It is obvious from *Figure* 7a that the before-exposure, cured film (*Figure* 7a lower spectrum) still contains a substantial amount of unreacted OH groups of the acrylic resin (3520 cm^{-1} band), and NH / OH (3380 cm^{-1}) and OCH_3 groups (2825 cm^{-1} and 910 cm^{-1}) of the melamine resin. The presence of these groups in the cured films affects both the photodegradation and hydrolysis of acrylic melamine coatings.

Because the coating films used in this study were relatively thick (≈10 mm), FTIR intensities of several strong absorption bands are substantial. However, except for the high extinction coefficient (κ) C=O band at 1730 cm^{-1} (κ = 0.36), our analyses of films having different thicknesses from 0.1 to 10 μm applied to both Si and CaF_2 substrates show little deviation from the Beer's absorption law (regression coefficients > 0.96). Thus, the use of thick films does not affect our ability to quantitatively monitor degradation. Instead, it allows us to detect and follow subtle changes in the low-IR absorbed groups and the appearance of new species produced during exposure.

Spectra recorded at different relative humidities before and after exposure time for a certain time, such as those shown in *Figure* 7a, may provide some information about the effects of RH on coating degradation. However, the effects are better accentuated by the difference spectra where the loss or gain of certain bands or the appearance of new bands can be readily discerned. Such FTIR difference spectra for samples exposed for 1278 hr at four different RH levels in the absence of UV light are illustrated in *Figure* 7b. These spectra were obtained by directly subtracting the spectrum of the unexposed specimen from the spectrum of the exposed specimen after adjusting for any

base line shift. The autosampler allows the spectra to be recorded at approximately the same location on each specimen. This operation minimizes errors due to sampling at different exposure times.

In the difference spectra of *Figure* 7b, the intensity of numerous bands in several regions, including 3050 to 2750 cm^{-1} and from 1600 to 900 cm^{-1}, decreases while the intensity in the 3100 to 3400 cm^{-1} and 1710 to 1580 cm^{-1} regions increases. Several new bands and shoulders also appear, including those near 3470, 3330, 3230, 1705, 1670, and 1630 cm^{-1}. The assignments of these bands are given in *Table* 1. Our analyses of amide model compounds and deuterium exchanges of amide model compounds and UV-degraded samples suggest that the band near 1670 cm^{-1} is due to the C=O of an amide and that the band around 1630 cm^{-1} is due to the NH deformation of a primary amine and / or a primary amide. D_2O treatment substantially reduces the 1630 cm^{-1} band intensity but has little effect on the 1670 cm^{-1} band. These assignments are consistent with those given in the literature for primary and secondary amines and amides and are supported by the fact that aliphatic secondary amines have no NH bending above 1470 cm^{-1}.[49]

It is interesting to note that the coating undergoes some changes even in the absence of UV and dry condition (<<1% RH / no UV), as evidenced by the decreases in the intensity of the bands between 3000 and 2800 cm^{-1} and 1600 and 900 cm^{-1} regions. These changes are probably caused by hydrolysis reactions during post curing. The water molecules required for this hydrolysis may have been supplied by a number of water-producing reactions taking place during curing or post curing, including the self-condensation reactions.[45,47]

It is evident from *Figure* 7b that, except for the 1340 cm^{-1} band, the intensity of all the bands formed or depleted increases with increasing RH. That is, an increase in RH results in an increase or a decrease of functional groups in the coatings. It should be noted here that, as mathematically expressed in the multilayer adsorption equation,[51] the amount of water sorbed in a material, hence the moisture content, is proportional to the relative vapor pressure of water, i.e., relative humidity (not to the partial water vapor pressure as sometimes erroneously stated in the literature). Therefore, although the moisture contents of the coatings at different RH levels were not measured in this study, the amounts of water in the films were expected to be greater at higher relative humidities.

Bauer[29] has used the reappearance of the acrylic resin OH band to follow the hydrolysis rate in the dark for a number of model acrylic melamine coatings exposed to water and noncondensing humidity. Further, he used the band at 915 cm^{-1} to measure the chain scission, and indicated that chain scission of this coating can be followed using the C–O–C bands at 915, 1015, or 1100 cm^{-1}. Using an FTIR correlation chart, we have demonstrated that the trends of the bands at 1015, 1085 (1100 cm^{-1} band in reference 29), and 1495 cm^{-1} are highly correlated so that tracking one of these bands is sufficient to follow degradation of a partially-methylated melamine coating.[24] For that reason, the 1085 cm^{-1} band is selected to measure the C–O bond loss of the coating during exposure in the absence and presence of UV light. However, it should be emphasized that the 1085 cm^{-1} band is due to the C–O bonds of both the acrylic-melamine crosslinks and the residual $-H_2C-O-CH_3$ groups of the melamine chains. Acid-catalyzed hydrolysis of this ether type is very complex, depending strongly on the level of substitution at the N atom of the melamine chains, which change with the degree of conversion,[52] and on the type and acidity of the solution.[39,52] No attempt is made to separate the contribution of each ether type in the coating used in this study. Thus, a change in the magnitude of the 1085 cm^{-1} band intensity is assumed to be due to a change in the C–O concentration of both the acrylic-melamine crosslinks and the melamine methoxy group. The formation of primary amines and amides is followed by the bands at 1630 and 1670 cm^{-1}, respectively.

Figures 8a and 8b show FTIR intensity changes with exposure time at different RH levels for the ether bond loss and primary amine formation, respectively, of samples exposed to 50°C in the absence of UV light. For material loss, it is more informative to express FTIR intensity decrease as the percentage of the intensity before exposure, as shown in *Figure* 8a. Coefficients of variation for the <<1% RH data, which were averaged of four specimens, were below 7%. No uncertainties are provided for the results at other relative

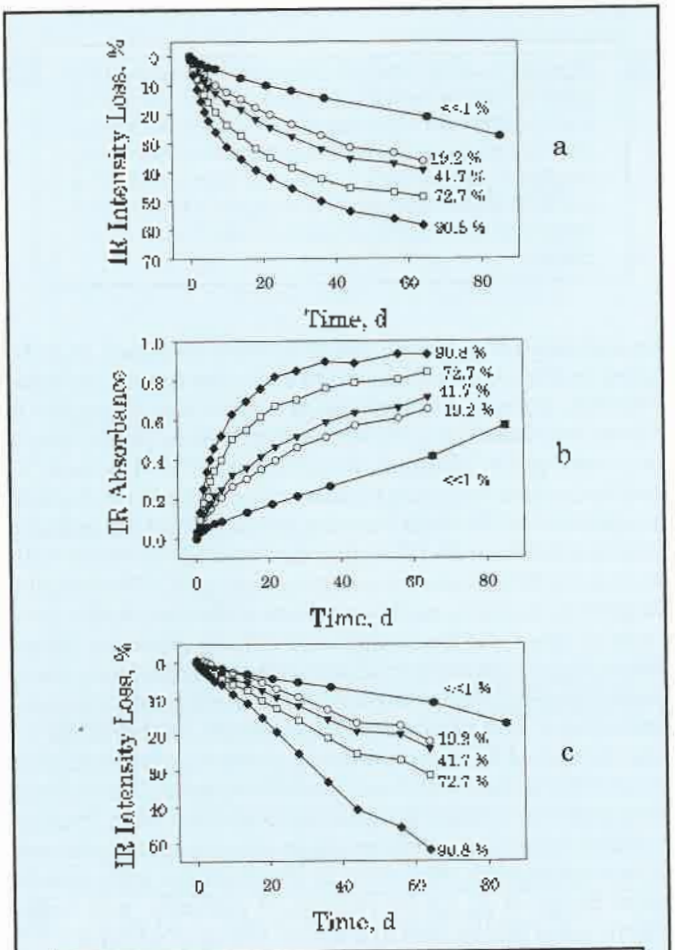

Figure 10—FTIR intensity changes as a function of exposure time for five different relative humidities at 50°C in the presence of "full UV": (a) C-O band at 1085 cm^{-1}, (b) Amide C=O band at 1670 cm^{-1}, and (c) Ester C–O band at 1170 cm^{-1}. (Error bars in the << 1% RH experimental data indicate one standard deviation.)

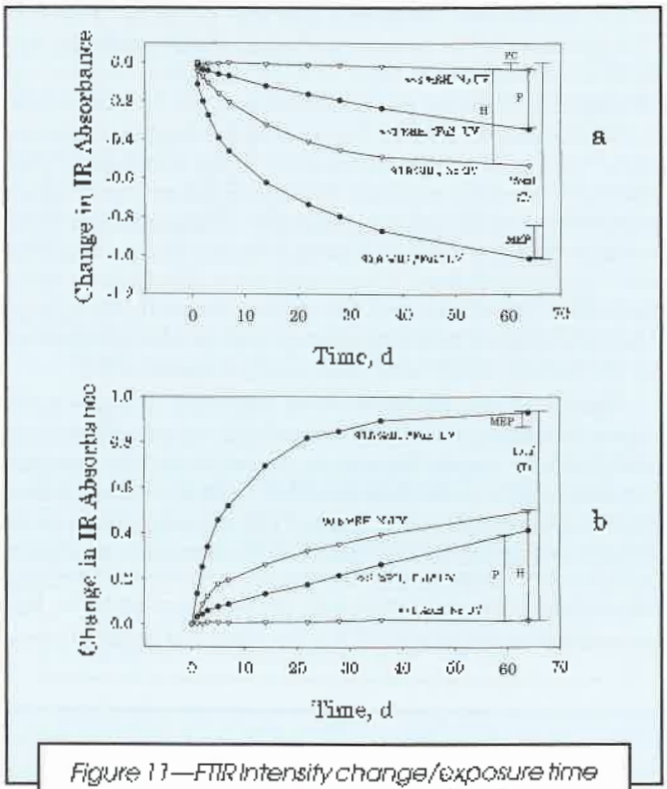

Figure 11—FTIR intensity change/exposure time plots to demonstrate the procedure for separating different degradation modes occurring during exposure to UV/humid environments: (a) material loss and (b) material formation. The vertical lines indicate the magnitude of each degradation mode at a particular UV/RH condition.

humidities because only one specimen was used, as indicated in the experimental section. In this figure, the total intensity increase or decrease at a particular humidity is due to the sum of hydrolysis reactions taking place during post curing (i.e., changes occurring at RH <<1% / no UV) and hydrolysis resulting from reactions of water in the film at a particular RH. Both the rates and extents of the primary amine formation and the ether loss initially increase with increasing RH. However, except for the <<1% RH where the degradation rate is nearly constant with time, hydrolysis rates at other RH levels decrease at long exposure times. Bauer[29] also observed a reduction in the hydrolysis rate of partially-alkylated melamine acrylic coatings at long exposure times, and attributed the decrease to the different reactivities of different methoxy groups in the melamine resin. That is, the most reactive methoxy groups hydrolyze first and less reactive groups are consumed later, leading to the slowing down of the reaction rate at longer exposures. This explanation, however, is inconsistent with results from Berge et al. for hydrolysis of partially- and fully-methylated melamines in alkaline and acid solutions.[52,53] Their results at various pH values do not show any evidence of a slow down with reaction time. Instead, the conversion of the partially-methylated material increases linearly with time. For the fully-methylated melamine, the hydrolysis rate in acid solutions even increases with reaction time. Fully-methylated melamines undergo little hydrolysis in alkaline solutions.[53]

In light of constant rate evidence provided by Berge et al.,[52,53] we believe that both the high rate at the early stage and the low rate at the late stage observed in *Figure* 8 may be explained by the heterogeneous nature of acrylic-melamine coatings. The cured film of this coating has a two-phase microstructure consisting of interstitial regions dispersed in a matrix.[54] The interstitial regions are believed to compose mostly low crosslinked, low molecular mass, polar materials, and the matrix contains mainly highly-crosslinked network units. The low molecular mass, low crosslinked regions are formed in coatings and polymers during film formation because, as the high molecular mass segments polymerize and terminate to form a network, some unreacted and partially-polymerized materials are unable to merge into the homogeneous structure and are left at the periphery of the network units.[55] These regions in an organic coating have been termed "D type" 56 or "hydrophilic" regions[57] because they behave like a hydrophilic membrane; that is, they take up a more substantial amount of water (45 to 75% mass fraction) and have an ionic diffusion coefficient several orders of magnitude greater than the rest of the film.[58] Corrosion of organic-coated steel has been observed directly beneath the D-type regions.[59] Such heterogeneous structure in polymers and coatings has been observed and widely reported.[55-62]

During exposure in humid environments, water enters the acrylic-melamine films predominantly at the hydrophilic sites, probably through both diffusion and osmotic-driven transport (due to the presence of hydrophilic materials). Hydrolysis likely occurs first at these hydrophilic locations. As degradation proceeds, the hydrolysis expands into the surrounding regions, perhaps through an acid autocatalytic process where the increased acidity is provided by the hydrolysis products.[54] Since hydrophilic regions are believed to contain mostly low molecular mass material, hydrolysis processes at these locations where water is more abundant than the surrounding network should be fast. Thus, the initial high degradation rate is attributed to the preferential hydrolysis in the hydrophilic regions of the films. Correspondingly, the lower rate at later exposure times is attributed to a depletion of hydrolyzable groups, low hydrolysis activity in the surrounding, nonhydrophilic regions, and a loss of material resulting from the hydrolysis (as evidenced by the CI loss shown in *Figure* 7b).

This explanation of heterogeneous degradation is supported by atomic force microscopy (AFM) analysis, which showed localized degradation on the surface of these samples during exposure to 70%RH / 50°C environment.[63] The local degraded areas deepened and enlarged (pitting) with exposure time. It is also consistent with similar pitting phenomenon observed by AFM in our laboratory for polyester hydrolysis in alkaline environments[64] and for polyurethane coatings exposed to different UV / RH conditions. In summary, we believe that hydrolysis of an acrylic-melamine coating initiates predominantly at the low molecular mass, hydrophilic regions of the film. And, although hydrolysis occurs in the hydrophilic regions throughout the film thickness, pits only form and enlarge from the hydrophilic areas near or on the surface.

Accelerated, inhomogeneous degradation has also been observed for acid-catalyzed hydrolysis of other polymeric systems. For example, using AFM in-situ measurement in

solution, Leadley et al.[64] have shown pit formation on the surface of poly(orthoester) films during water immersion. Once formed, these pits broadened and deepened relatively quickly. Similarly, Gopferich and Langer[65] have observed pore formation and deepening in polyanhydrides exposed in neutral solutions. Using pH-sensitive dye in combination with fluorescence scanning confocal microscopy, they were able to measure pH as a function of pore depth. They observed a gradual decrease of pH from a value of 7.4 in the exposed solution to 5.75 at the depth of approximately 200 μm from the pore surface. Recent tapping mode AFM study by Gu et al.[66] has also shown that the base-catalyzed hydrolysis of polyesters is also an heterogeneous process, with pits forming at certain sites followed by rapid enlargement and deepening at these sites.

Based on FTIR spectral results given in *Figure 7*, the loss of the ether bonds (1085 cm^{-1} band) and the formation of primary amines (1630 cm^{-1} band) of a partially-methylated melamine acrylic coating exposed to moisture in the absence of UV light probably occur by the following pathways:

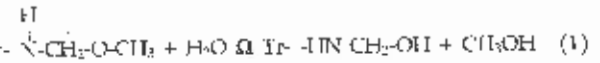

$$Tr\text{-}\overset{H}{\underset{|}{N}}\text{-}CH_2\text{-}O\text{-}CH_3 + H_2O \;\Omega\; Tr\text{-}HN\text{-}CH_2\text{-}OH + CH_3OH \quad (1)$$

$$Tr\text{-}\overset{H}{\underset{|}{N}}\text{-}CH_2\text{-}O\text{-}R + H_2O \;\Omega\; Tr\text{-}HN\text{-}CH_2\text{-}OH + ROH \quad (2)$$

$$Tr\text{-}N(CH_2\text{-}O\text{-}CH_3)_2 + H_2O \;\Omega\; Tr\text{-}N(CH_2OH)_2 + CH_3OH \quad (3)$$

$$Tr\text{-}N(CH_2\text{-}O\text{-}R)_2 + H_2O \;\Omega\; Tr\text{-}N(CH_2OH)_2 + ROH \quad (4)$$

where Tr is the triazine ring and R is the acrylic resin chain; the compounds in the left-hand side of Reactions 1 to 4 are the possible materials present in the cured film, as presented in *Figure 1*.

It is likely that the products of Reactions 3 and 4 undergo further hydrolysis to form two methylol groups per melamine chain[52]:

$$Tr\text{-}N(CH_2OH)(CH_2O\text{-}R) + H_2O \;\Omega\; Tr\text{-}N(CH_2OH)_2 + ROH \quad (5)$$

Reaction 5 has been found to be faster than Reaction 4, presumably the addition of a proton to the ether oxygen is

Figure 12—Bar chart plots showing the effect of relative humidity on the magnitude of post curing, hydrolysis, photodegradation, and moisture-enhanced photodegradation of specimens exposed for 14 days in the presence of "full UV" at 50°C; (a) ether bond loss, (b) amide C=O formation, and (c) ester side chain cleavage.

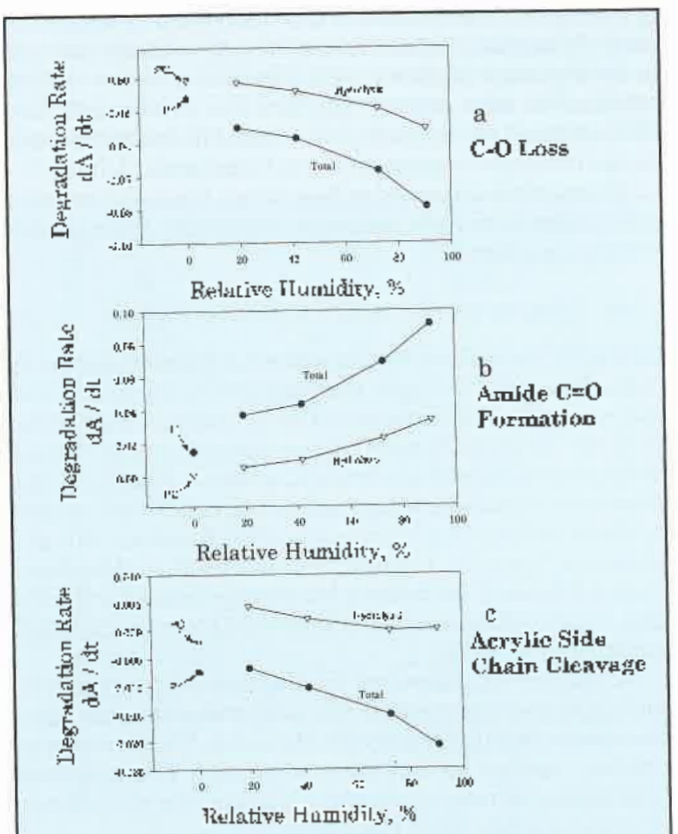

Figure 13—Degradation rate (dA/dt) as a function of relative humidity for total degradation, hydrolysis, and moisture-enhanced photodegradation of a partially-methylated melamine acrylic coating exposed to "full UV" light at 50°C; (a) ether bonds loss and (b) amide C=O formation, and (c) ester side chain cleavage. (Values for P and PC are indicated with the arrows.)

Table 2—Rates (dA/dt) of Total Degradation, Hydrolysis, and Moisture-Enhanced Photodegradation for Three Functional Groups in a Partially-Methylated Melamine Acrylic Coating Exposed to "Full UV" at 50°C for Three Relative Humidities

	<<1% RH	19.2% RH			90.8% RH		
Functional Group	T=(P)	T	H	MEP	T	H	MEP
Amide C=O formation, 1670 cm^{-1}	0.015 ± 0.002	0.037	0.071	0.022	0.092	0.061	0.062
Ether Bond Loss, 1085 cm^{-1} [a]	-0.012 ± 0.003	-0.030	-0.008	-0.019	-0.078	-0.063	-0.037
Acrylic Ester Cleavage, 1170 cm^{-1}	-0.007 ± 0.001	-0.007	0.004	-0.005	-0.02	0.002	-0.033

(a) Negative values indicate loss of material and the numbers after the ± symbol are the standard uncertainty.

easier when one methylol group is present than when both are alkoxylated. Reactions 1 to 5 are believed to be the main hydrolysis routes that account for the loss of the ether band at 1085 cm^{-1} to form melamine methylols and also to reform the starting acrylic resin. These reactions proceed by protonation of the ether oxygen atom.

The methylols formed in Reactions 1 and 2, being primary alcohols, oxidize readily (deformylate) to form primary amines and aldehydes according to Reaction 6[67]:

$$\text{Tr-}\cdot\text{HN-}\cdot\text{CH}_2\text{-OH (from Rx 1 and 2)} \rightarrow \underset{\text{fast}}{\text{Tr-}\cdot\text{NH}_2}\text{+CH}_2\text{O} \quad (6)$$
(Primary amine, 1630 cm^{-1})

In this case, the methylol group is activated by the addition of a proton to the N-atom in the side group to which the methylol is attached. Since formaldehyde molecules formed in the exposure chamber were either removed or readily oxidized to form acids,[34] Reaction 6 is irreversible. The disubstituted amino methylols formed in Reactions 3 to 5 do not undergo decomposition to form formaldehyde.[32]

The methylols formed in Reactions 1 through 5 can also self-condense to form melamine-melamine linkages following Reaction 7[29]:

$$\text{Tr-}\cdot\text{NCH}_2\text{OH} \rightleftarrows \text{Tr-N-}\cdot\text{CH}_2 \quad \text{N Tr} - \text{H}_2\text{O} - \text{CH}_2\text{O} \quad (7)$$

However, we believe that Reaction 6 is the main pathway in the absence of UV light, as evidenced by the substantial increase in the FTIR intensity of the primary amine band at 1630 cm^{-1} (*Figures* 7b and 8). The temperature of 50°C used in this study should accelerate Reaction 6. Reaction 7 is a minor reaction under our experimental conditions, as seen by the small increase in intensity of the band at 1340 cm^{-1} shown in *Figure* 7b. Volatile products produced by Reactions 1, 3, 6, and 7 are believed to be responsible for the CH loss, which can be seen in the 2800 to 3000 cm^{-1} region (CH stretch) of *Figure* 7b.

A number of pathways for the hydrolysis of acrylic melamine coatings, several of which produce amines, have been presented in reference 29. However, the formation of primary amines has not been discussed. The proposed hydrolysis pathways to form the 1705 cm^{-1} band (carboxylic acids) are described elsewhere.[31]

Effects of Relative Humidity on Degradation in the Presence of UV Light

FTIR difference spectra of samples exposed to different RH levels at 50°C in the presence of "full UV" are displayed in *Figure* 9. The thickness of these samples is similar to that for *Figure* 7, i.e, 10 $\mu m \pm 1.2$ μm. In the absence of UV radiation, the coating shows only small changes under dry condition (<<1% RH) (*Figure* 8). However, it undergoes substantial degradation during exposure to "full UV" light at the same RH and temperature. Intensity increases in the 3100 to 3650 cm^{-1} region and formation of the bands at 1760, 1670 and 1630 cm^{-1} are observed. The 1630 and 1670 cm^{-1} bands have already been assigned to the NH bending of primary amines and amides and C=O stretching of amides, respectively. The compound responsible for the C=O band at 1760 cm^{-1}, which is quite sensitive to RH change, is not known. Lemaire and Siampiringue[17] have attributed the bands occurring in the 1750 to 1850 cm^{-1} region during photodegradation of acrylic melamine materials as due to anhydrides. Anhydrides have also been observed as one of the photodegradation products of acrylic polymers.[68] However, the 1760 cm^{-1} band in *Figure* 9 does not appear to be of an anhydride because an acid anhydride C=O usually has two peaks near 1760 and 1820 cm^{-1}. Bauer and Briggs[21] have suggested a band at 1770 cm^{-1} in the spectra of photodegraded acrylic-melamine coatings as due to peracid/perester formation.

The intensities of numerous bands associated with the melamine-acrylic structure decrease with dry UV exposure, including those at 1495, 1085, and 1380 cm^{-1}. Further, the intensities of the bands associated with the acrylic resin portion, e.g., at 1730 cm^{-1}, due to ester C=O, and at 1170 cm^{-1}, due to ester C-O, which are only slightly affected by the <<1% RH/no-UV condition, also decrease substantially during <<1% RH/UV exposure. The formation of amines and various carbonyl-containing compounds (*Figure* 9) in samples exposed to <<1% RH/"full UV" condition is consistent with the photodegradation pathway proposed by Lemaire[17] for acrylic melamine coatings. Loss of the ester C–O bonds of the acrylic resin portion is in agreement with previous observations that photodegradation of polyacrylates[68] and poly(methyl methacrylate)[69] at ambient temperature (25°C) primarily results in the cleavage of the ester side chains.

A comparison of the spectral characteristics given in *Figures* 7 and 9 reveals substantial differences in both the magnitude and pathway of the degradation between the absence and presence of UV. Differences in the extent of degradation can be seen in the intensity losses of the CH band at 2960 cm^{-1} and the C–O band at 1085 cm^{-1}; both of which show a more severe degradation in the presence of UV than in its absence. AFM images from the same coating also showed broader, deeper, and a greater number of pits formed in samples exposed to UV than in those not exposed to UV.[63] Changes in the degradation pathway are evidenced from the line shapes of the FTIR bands in the 3600 to 3100 cm^{-1} and 1700 to 1600 cm^{-1} regions. For example,

the 1670 cm^{-1} band, which appears only as a shoulder near the 1630 cm^{-1} band under no UV (*Figure* 7b), becomes pronounced with UV. The relative intensity of the 1670 cm^{-1} band with respect to the 1630 cm^{-1} band with exposure time also increases markedly under UV. Further, the intensities of the acrylic resin bands, e.g., at 1730 cm^{-1} and at 1170 cm^{-1}, also increase substantially in the presence of UV as compared to exposure in the dark at the same RH.

The effects of RH on the degradation of a partially-methylated melamine coating exposed to 50°C in the presence of the "full UV light" are displayed in *Figure* 10. This figure depicts FTIR intensity changes of the bands at 1085 cm^{-1} (ether bond loss), 1670 cm^{-1} (amide C=O formation), and 1170 cm^{-1} (acrylic side chain cleavage) as a function of exposure time. As in the absence of UV light, material loss (*Figures* 10a and 10c) is expressed as percentage of IR intensity decrease with respect to the initial intensity. Again, values for the <<1% RH are averaged from four specimens and values at other RH levels are from one specimen. The coefficients of variation for the <<1% RH data are below 5%. As an indication of the reproducibility of the results, one standard deviation error bars are drawn for experimental data points for << 1% RH results of *Figure* 10. *Figure* 10 shows several main results: (1) both the rate and extent of degradation are much greater in humid environments than in dry environment, (2) the extent and early rate of degradation in the presence of UV radiation increase with increasing RH, and (3) degradation under a dry condition in the presence of UV light increases nearly linearly with exposure time, but the rates of both the amide C=O formation and ether loss at relative humidities greater than 19.2% are high at first and then level off with exposure time. This rate change behavior with exposure time for the ether loss is similar to that in the absence of UV (see *Figure* 8).

Figure 10 also reveals that, as with the bands associated with the melamine structure, the rate of acrylic side chain cleavage (band 1170 cm^{-1}, *Figure* 10c) at short exposure times increases with increasing RH. However, instead of leveling off at later exposure times, as observed for the ether bond loss of the melamine-acrylic structure and melamine chains, the acrylic resin side chain cleaves at a nearly constant rate with time. The leveling off of the chemical groups associated with the acrylic-melamine structures or melamine chains (e.g., C–O at 1085 cm^{-1}) has been explained as a result of coatings heterogeneity. However, the reason for the constant degradation rate for the UV-exposed acrylic resin portion is not known. One possible explanation is that the photodegradation of the acrylic polymer may follow an autocatalytic process; that is, once radicals have been formed in the acrylic chains, they continue to propagate or transfer to other chains until the degradation is complete. Direct evidence for this postulation is not available. However, it has been shown that photolytic cleavage of the ester side chain of polyacrylates and poly(methyl methacrylate) has a high quantum efficiency and that the photodegradation rate of these materials remains constant with time.[67,68]

Data on photodegradation of polyacrylate and polymethacrylate polymers (two components of the acrylic resin used in this study) in the presence of relative humidity or water is not available. However, the effect of moisture on photodegradation of polycarbonate has been reported.[15] The presence of water affects neither the reaction rates nor the mechanisms but does decrease the activation energy of the photoFries rearrangement (which results in C–O bond scission) of this polymer. The activation energy lowering by water of polycarbonate is believed to be due to the greater stabilization of the transition state compared with the parent excited state. Such extra stabilization occurs because a weakening of the C–O bonds allows the oxygen of the C–O group to form a stronger hydrogen bond with water.

Relative Contributions of Photodegradation, Hydrolysis, and Moisture-Enhanced Photodegradation

Total FTIR intensity changes at any RH / UV combination as shown in *Figure* 10 are the result of contributions from four different degradation modes: (1) reactions occurring during exposure in dry condition (<<1% RH) in the absence of UV light, (2) hydrolysis in the dark due to water in the film at a particular relative humidity, (3) photodegradation (photo-induced degradation in the absence of moisture), and (4) moisture-enhanced photodegradation. The experiments were designed to isolate the relative contribution to the total degradation from each degradation mode.

Examples to illustrate the procedure used for separating the total degradation into four separate modes are presented in *Figures* 11a and 11b for the depletion and formation, respectively, of chemical groups in the film. These figures portray the total FTIR intensity (T) changes with

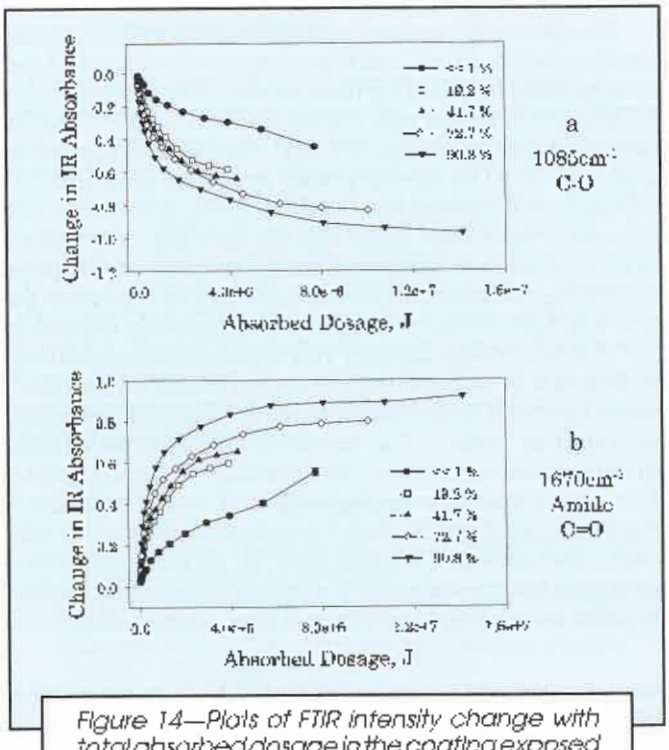

Figure 14—Plots of FTIR intensity change with total absorbed dosage in the coating exposed to five different relative humidities in "full UV" at 50°C: (a) ether bonds loss and (b) amide C=O formation. The apparent quantum yields are obtained from the initial slopes. (Error bars in the << 1% RH experimental data indicate one standard deviation.)

exposure time for the 1085 and 1670 cm^{-1} bands of samples exposed to <<1% RH and 90.8% RH in the presence and absence of UV. The curve for the <<1% RH / no-UV condition represents hydrolysis reactions due to post-curing in the absence of light; this post-cure degradation is designated as PC. The curve for the 90.8% RH / no-UV condition, designated as H, consists of PC and hydrolysis in the dark at 90.8% RH. The hydrolysis in the dark at 90.8% RH is then the difference between these two curves. Similarly, data for the <<1% RH / "full UV" condition comprised of PC and photodegradation (P); and the difference between that set of data and the set for <<1% RH / no-UV yields the results for P at <<1% RH in "full UV." Finally, the contributions due to moisture-enhanced photodegradation (MEP) at 90.8% RH under "full UV" is the difference between the total degradation (T) and the sum of PC, P, and H at 90.8% RH. Similar analysis is applied to obtain data for other UV / RH conditions.

Figures 12a, 12b, and 12c show the influence of RH on the extent of each of the four degradation modes for the ether bond loss, amide C=O formation, and acrylic ester side chain cleavage, respectively. These results are obtained after 14-days exposure, which is selected to minimize complications due to possible changes in the degradation modes at longer exposure times. In these figures, the contributions to the total degradation at <<1% RH / "full UV" are PC and P, while the contributions at other RH / "full UV" conditions consist of PC, P, H, and MEP. As seen in this figure, except for the small differences between values obtained for 19.2% RH and 41.7% RH for ether loss and amide formation, the magnitudes of T, H, and MEP increase with increasing RH.

The effect of RH on the degradation rates of ether loss and amide formation for T and H are displayed in *Figure* 13 and summarized in *Table* 2 for three relative humidities. *Figure* 13 also provides the rate values for the P and PC modes (arrowed data points near 0% RH). The rate is expressed as a change in FTIR intensity with exposure time (dA/dt, where A is IR absorbance and t in d for days). The rate values of H and T are taken directly from the initial slopes of the curves given in *Figures* 8 and 10, respectively. Because the PC degradation rate is small, the rate of T given at the <<1% RH condition in the table is considered as due solely to P. Consequently, the MEP rate at each relative humidity is obtained by subtracting the sum of H and P from the T value for that RH. The rates of MEP for three RH levels are included in *Table* 2. The results for all three functional groups presented in *Figure* 13 show that the total degradation rate is greater than that of PC, H, and P combined. Further, except for the dark hydrolysis of the acrylic side chain, the rates of T, H, and MEP for all three functional groups in the presence of UV increase with increasing RH. It is also interesting to note from *Figure* 13c that, despite no dark hydrolysis taking place in the acrylic polymer chains, moisture plays a vital role in the total degradation of the acrylic resin structure of a partially-methylated melamine acrylic coating exposed to humid / UV environment. These results suggest that products from the hydrolysis of acrylic-melamine and melamine structures or / and plasticization of moisture contribute to the moisture-enhanced photodegradation of the acrylic polymer chains.

The results of *Figure* 13 or *Table* 2 allow one to conveniently estimate relative degradation rates as a function of RH for different degradation modes. For example, the relative T / P rate for the amide formation at 19.2% RH is 0.037 / 0.015 and at 90.8% RH is 0.092 / 0.015. This means that the total rate of the amide formation at 19.2% RH is only 2.4 times greater than the photodegradation rate alone but is more than six times greater at 90.8% RH. These results indicate that moisture in the film accelerates the oxidation and that the magnitude of the oxidation increases with increasing RH. Similarly, the rate of ether loss due to hydrolysis is only approximately two-thirds of that of the photodegradation at 19.2% RH, but is more than five times greater than that of P at 90.8% RH. This behavior points to the importance of hydrolysis in the total degradation of this coating when it is exposed to water or high relative humidities. It is clear from *Figure* 12 that the relative contributions of both the rate and magnitude of P and H to the total degradation depend strongly on the level of RH in the exposure environment.

Effects of Relative Humidity on Apparent Quantum Yield

Figures 14a, 14b, and 14c display ether loss, amide C=O formation, and ester side chain cleavage, respectively, as a function of total absorbed dosage for specimens exposed at different relative humidities in "full UV" at 50°C. The total absorbed dosage, i.e., the actual amount of radiation absorbed in the coating, is calculated following the scheme of *Figure* 3 and equation 2. As in the case of damage / time relation (*Figure* 10), the damage / dosage plot indicates that humid / UV conditions cause greater degradation in the coatings than did the dry / UV condition. However, the damage / dosage curves show less discernable effect between the RH levels from 19.2% and 90.8% than the damage / time plots.

The apparent quantum yield is determined from the initial portion of the slope of the damage / dosage curve to avoid complications from multiple degradation modes and from shielding of the coating material by degradation products absorbing radiation. We have fitted the damage / dosage relationship using a fourth-order polynomial function to provide the quantum yield. We have, for conve-

Table 3—Apparent Quantum Yields (Am-1J-1) as a Function of Relative Humidity for Several Functional Groups of a Partially-Methylated Acrylic Melamine Coating Exposed to "Full UV" at 50°C

Functional Group	Relative Humidity			
	<<1%	19.2%	72.7%	90.8%
Amide C=O formation, 1670 cm^{-1}	$(9.3 \pm 2.3) \times 10^{-6}$	4.7×10^{-7}	4.9×10^{-7}	5.2×10^{-7}
Ether bond Loss, 1085 cm^{-1}	$(7.3 \pm 0.18) \times 10^{-6}$	3.6×10^{-7}	3.8×10^{-7}	4.1×10^{-7}
Acrylic ester cleavage, 1170 cm^{-1}	$(1.4 \pm 0.8) \times 10^{-6}$	3.7×10^{-6}	4.0×10^{-6}	4.4×10^{-6}

nience, arbitrarily estimated the quantum yield from the slope of the curve extending from zero absorbed dosage to 2.0×10^{-6} J. Apparent quantum yields for the amide C=O formation, ether bond loss, and ester side chain cleavage of a partially-methylated melamine acrylic coating at different relative humidities are given in *Table* 3. The apparent quantum yields in humid environments are greater than that in dry environment, and there appears a slight increase of quantum yield with an increase in relative humidity.

Since the unit used to express the apparent quantum yield in this study is different from that traditionally used (i.e., number of molecules undergo change / number of quanta absorbed), the values obtained here should not be used to compare with the quantum yield results reported in the literature for polymers. Work is in progress to measure the molar absorption coefficients of the IR bands of interest. The results will be used to convert IR absorbance units into chemical functionality concentrations.

Nevertheless, quantum efficiencies of chain scission in polymers in the solid state are generally very low, varying from 10^{-4} for poly(ethylene terephthalate) irradiated with a 280 nm to 360 nm light source to 10^{-2} for poly(methyl methacrylate) irradiated at 253.7 nm.[10] Both the temperature and the state (e.g., solid, liquid) of polymers have a strong effect on the quantum yield. For example, the quantum yield of polycarbonate irradiated in solution was found 40 times greater than that in solid state.[7] Dan and Guillet[12] also reported that quantum yield of the chain scission in glassy polymers increases rapidly to the value obtained for the same polymer in solution as the temperature is increased to above the glass transition temperature. The only available data on the effect of moisture on the quantum efficiency of polymers is from the work of Gupta et al.,[13] who reported a change of quantum yield from 0.005 ± 0.002 at 0% RH to 0.007 ± 0.003 at 100% RH for polycarbonates exposed to 300 to 400 nm wavelength radiation at 26°C.

This study covered a wide range of RH from <<1% to 90% at 50°C. Therefore, the results on the effects of relative humidity on the photodegradation and quantum yields can be applied to atmospheric weathering of partially-methylated melamine acrylic coatings if the outdoor environments are carefully characterized. For hydrolysis in the dark, to correlate the data obtained from this study with outdoor exposure, both the temperature and RH of the atmosphere immediately above the surface of the outdoor sample must be continuously recorded. In this case, the time of the sample in the dark can be used as the parameter for the correlation. In the presence of UV light, the correlation between outdoor and indoor is only possible if the total dosage absorbed in the outdoor sample is measured. In this case, the absorbed dosage must be used as the denominator because weather elements constantly change during the time of the day and season of the year, making time a useless parameter for relating outdoor and indoor data.

CONCLUSIONS

The effects of relative humidity from <<1% to 90% on the photodegradation and quantum yield for a partially-methylated melamine acrylic coating exposed to "full UV" at 50°C are reported. The following conclusions are made:

(1) In humid environments with or without UV radiation, the degradation of partially-methylated melamine acrylic coatings occurs rapidly in the early stage but levels off at long exposure times. This degradation behavior is explained by the inherently heterogeneous microstructure of the coating; degradation at the early stage occurs mostly in the "hydrophilic" regions of the film.

(2) The total degradation in the presence of UV is caused by four different modes: reactions during post-curing, hydrolysis at a particular RH, photodegradation, and moisture-enhanced photodegradation. Experiments were designed so that the effect of RH on each mode was isolated.

(3) The magnitude and early rate of the total degradation, hydrolysis, and moisture-enhanced photodegradation increase with increasing RH.

(4) The contribution of each mode to the total degradation varies with RH. At low RH levels, photodegradation is an important mode; however, at high relative humidities, the hydrolysis mode accounts for the majority of the total degradation.

(5) Moisture in the film enhances the apparent quantum efficiency of photodegradation of acrylic melamine coatings.

(6) Based on spectroscopic evidence, the degradation of a partially-methylated acrylic coating exposed to moist environments in the absence of UV light is believed to occur by first hydrolyzing the coating crosslinks and melamine methoxymethyl groups to form methylol compounds, followed by the decomposition of the primary methylols to produce primary amines and formaldehyde.

ACKNOWLEDGMENTS

The research reported here is part of a government / industry / university consortium on Service Life Prediction at NIST. Companies involved in this consortium include Akzo Nobel, Atofina, Atlas Electric Devices Inc., Dow Chemical, DuPont Automotives, Durom Inc., Eastman Chemicals, Millennium Inorganic Chemicals, PPG, and Sherwin Williams Co. Federal Highway Administration, Wright Patterson AFB, and Forest Products Laboratory also provided additional funds for this research. We also thank Dr. Brian Dickens for his assistance in the automation of data analysis, Dr. Walt Meyer of DuPont for providing the model acrylic resin, and Cytec Industries for providing the Cymel 325 resin.

References

(1) Burroughs, W.J., *Weather Cycles: Real or Imaginary*, Cambridge University Press, New York, 1992.
(2) Martin, J.W., Saunders, S.C., Floyd, F.L., and Wineburg, J.P., "Methodologies for Predicting the Service Life of Coatings," *Federation Series on Coatings Technology*, Federation of Societies for Coatings Technology, Blue Bell, PA, 1996.
(3) Norins, A.L., in *The Biological Effects of Ultraviolet Radiation*, Urbach, F. (Ed.), Pergamon Press, New York, p. 605, 1969.
(4) Scotto, J. and Fears, T.R., *Cancer Invest.*, 5, 275 (1987).
(5) Caldwell, M.M., *Photophysiol.*, 6, 131 (1971).
(6) Hirt, R.C., Schmitt, R.G., Searle, N.D., and Sullivan, A.P., *J. Opt. Soc. Am.*, 50, 706 (1960).
(7) Zerlaut, G.A. and Ellinger, M.L., *J. Oil & Colour Chemists' Assoc.*, 64, 387 (1981).
(8) Zerlaut, G.A., in *Accelerated and Outdoor Durability Testing of Organic Materials*, Kelola, W.D. and Grossman, D. (Eds.), ASTM

STP 1202, American Society for Testing and Materials, Philadelphia, PA, p. 1, 1993.
(9) Randy, B. and Rabeck, J.F., *Photodegradation, Photooxidation and Photostabilization of Polymers: Principles and Applications*, John Wiley and Sons, New York, p. 6, 1975.
(10) Rabek, J.F., *Polymer Photodegradation-Mechanisms and Experimental Methods*, Chapman and Hall, New York, pp 1-66, 1995.
(11) Guillet, J.E., Li, S.K.L., and Ng, H.C., *Am. Chem. Soc. Symp. Series 266*, American Chemical Society, Washington, D.C., p. 165, 1984.
(12) Dan, E. and Guillet, J.E., *Macromolecules*, 6, 230 (1973).
(13) Gupta, A., Rembaum, A., and Moacanin, J., *Macromolecules*, 11, 1285 (1978).
(14) Martin, J.W., Nguyen, T., Byrd, E., Embree, N., and Dickens, B., *Polym. Deg. Stab.*, 75, 193 (2002).
(15) Bauer, D.R., Gerlock, J.L., and Mielewski, D.F., *Polym. Deg. and Stab.*, 36, 9 (1992).
(16) Bauer, D.R., "Chemical Criteria for Durable Automotive Topcoat," Journal of Coatings Technology, 66, No. 835, 57 (1994).
(17) Lemaire, J. and Siampiringue, N., in *Service Life Prediction of Organic Coatings, A Systematic Approach*, Bauer, D. and Martin, J.W. (Eds.), ACS Symposium Series 722, American Chemical Society, Washington, D.C., p. 246, 1999.
(18) Carduner, K.R., Carter, R.O. III, Zinbo, M., Gerlock, J.L., and Bauer, D.R., *Macromolecules*, 21, 1598 (1988).
(19) Gerlock, J.L., Mielewski, D.F., Bauer, D.R., and Carduner, K.R., *Macromolecules*, 21, 1604 (1988).
(20) Lamers, P.L., Johnston, B.K., and Tyler, W.H., *Polym. Deg. Stab.*, 55, 309 (1997).
(21) Bauer, D.R. and Briggs, L.M., in *Characterization of Highly Crosslinked Polymers*, Labana, S.S. and Dickie, R.A. (Eds.), ACS Symposium Series 243, American Chemical Society, Washington, D.C., p. 271, 1983.
(22) Bauer, D.R. and Mielewski, D.F., *Polym. Deg. Stab.*, 40, 349 (1993).
(23) Weast, R. (Ed.), *Handbook of Chemistry and Physics*, 53rd ed., CRC Press, p. D148, 1972.
(24) Gerlock, J.L., Van Oene, H., and Bauer, D.R., *Euro. Polym. J.*, 19, 11 (1983).
(25) Gerlock, J.L., Dean, M.J., Korniski, T.J., and Bauer, D.R., *Ind. Eng. Chem. Prod. Res. Dev.*, 25, 449 (1986).
(26) English, A.D. and Spinelli, H.J., in *Characterization of Highly Crosslinked Polymers*, Labana, S.S. and Dickie, R.A. (Eds.), ACS Symposium Series 243, American Chemical Society, Washington, D.C., p. 257, 1984.
(27) English, A.D. and Spinelli, H.J., "Degradation Chemistry of Primary Crosslinks in High Solids Enamel Finishes: Solar Assisted Hydrolysis," Journal of Coatings Technology, 56, No. 711, 43 (1984).
(28) Nguyen, T., Martin, J.W., Byrd, E., and Embree, N., *Polym. Deg. Stab.*, 77, 1 (2002).
(29) Bauer, D.R., *J. Appl. Polym. Sci.*, 27, 3651 (1982).
(30) Rodgers, W.R., Garner, D.P., and Chuever, C.D., "Study of the Attack of Acidic Solutions on Melamine-Acrylic Basecoat/Clearcoat Paint Systems," Journal of Coatings Technology, 70, No. 877, 83 (1998).
(31) Mori, K., Tachi, K., Muramatsu, M., and Torita, K., in *Proc. XXIV Pattpec Congress*, A, p. 101, 1998.
(32) Schulz, U., Trubiroha, P., Schermau, U., and Baumgart, H., *Prog. Org. Coat.*, 40, 151 (2000).
(33) Wernstäh, K.L., *Polym. Deg. Stab.*, 54, 57 (1996).
(34) Holubka, J.W., Schmitz, P.J., and Xu, Li-F., "Acid Etch Resistance of Automotive Clearcoats. I: Laboratory Test Method Development," Journal of Coatings Technology, 72, No. 901, 77 (2000).
(35) Praue, J.A., "Introduction to Polymers and Resins," *Federation Series on Coatings Technology*, Federation of Societies for Coatings Technology, Philadelphia, PA, 1986.
(36) Rancourt, J.D., *Optical Thin Films, User's Handbook*, McGraw-Hill, New York, p. 183, 1987.
(37) Bauer, D.R., *Prog. Org. Coat.*, 23, 105 (1993).
(38) Johnson, B.W. and McIntire, R., *Prog. Org. Coat.*, 27, 95 (1996).
(39) Decker, C. and Bendaikha, T., in *Int. Conf. Adv. Stab. and Controlled Deg. Polymers*, Patsis, A. (Ed.), Technomic, Lancaster, PA, p. 143, 1989.
(40) Decker, C., Moussa, K., and Bendaikha, T., *J. Polym. Sci., Polym. Chem.*, 29, 739 (1991).
(41) Costa, G.W., Hirt, R.C., and Smalley, D.I., *J. Chem. Phys.*, 18, 434 (1950).
(42) Fox, R.B., Isaacs, L.G., Stokes, S., and Kagarise, J., *J. Polym. Sci.*, A1, 2085 (1964).
(43) Bauer, D.R., *Prog. Org. Coat.*, 14, 193 (1986).
(44) Chang, T.T., *Prog. Org. Coat.*, 29, 45 (1996).
(45) Blank, W.J., "Reaction Mechanism of Melamine Resins," Journal of Coatings Technology, 51, No. 656, 61, (1979).
(46) Santer, J.O., *Prog. Org. Coat.*, 12, 309 (1984).
(47) Bauer, D. and Dickie, R., *J. Appl. Polym. Sci.*, 18, 2014 (1980).
(48) Larkin, P.J., Makowski, M.P., Colthup, N.B., and Flood, L.A., *Vibrational Spectros.*, 17, 53 (1998).
(49) Colthup, N.B., Daly, L.H., and Wiberley, S.E., *Introduction to Infrared and Raman Spectroscopy*, 3rd ed., Academic Press, New York, p. 439, 1990.
(50) Samaraweera, U. and Jones, F.N., "Possible Reaction Pathways for Self-Condensation of Melamine Resins; Reversibility of Methylene Bridge Formation," Journal of Coatings Technology, 64, No. 804, 69 (1992).
(51) Adamson, A.W., *Physical Chemistry of Surfaces*, 2nd ed., Interscience, New York, p. 585, 1967.
(52) Berge, A., Kvaeven, B., and Ugelstad, J., *European Polym. J.*, 6, 981 (1970).
(53) Berge, A. Gudmundsen, S., and Ugelstad, J., *European Polym. J.*, 5, 171 (1969).
(54) Nguyen, T., Martin, J.W., Saunders, S., and Byrd, E., "Modes, Mechanism and Model for Hydrolysis of Acrylic-Melamine Coatings in the Absence of UV Light," *Proc. 75th Annual Meeting of the Federation of Societies for Coatings Technology*, Atlanta, GA, November, pp. 759-796, 2001.
(55) Bascom, W.D., *J. Adhesion*, 2, 168 (1970).
(56) Mayne, J.E.O. and Mills, D.J., *J. Oil & Colour Chemists' Assoc.*, 58, 155 (1975).
(57) Nguyen, T., Hubbard, J.B., and Pommersheim, J.M., "Unified Model for the Degradation of Organic Coatings on Steel in a Neutral Electrolyte," Journal of Coatings Technology, 68, No. 855, 45 (1996).
(58) Corti, H., Fernandez-Prini, R., and Gomez, D., *Prog. Org. Coat.*, 10, 5 (1982).
(59) Mills, D.J. and Mayne, J.E.O., in *Corrosion Control by Organic Coatings*, Leidheiser, H. Jr., (Ed.), Nat. Assoc. Corr. Eng., Houston, TX, p. 12, 1981.
(60) Cuthrell, R.E., *J. Appl. Polym. Sci.*, 12, 1263 (1968).
(61) Kuryakina, M.I. and Kuzmak, A.E., *Prog. Org. Coat.*, 18, 325 (1990).
(62) VanLandingham, M.R., Eduljee, R.F., and Gillespie, J.W. Jr., *J. Appl. Polym. Sci.*, 71, 699 (1999).
(63) VanLandingham, M., Nguyen, T., Byrd, E., and Martin, J.W., "On the Use of the Atomic Force Microscope to Monitor Physical Degradation of Polymeric Coatings Surfaces," Journal of Coatings Technology, 73, No. 923, 43 (2001).
(64) Headley, S.R., Shakesheff, K.M., et al., *Biomaterials*, 19, 1353 (1998).
(65) Gopferich, A. and Langer, R., *J. Polym. Sci., Part A, Polym. Chem.*, 31, 2445 (1993).
(66) Gu, X., Raghavan, D., Nguyen, T., and VanLandingham, M., *Polym. Deg. Stab.*, 74, 139 (2001).
(67) Streitwieser, D. Jr. and Heatcock, C.H., *Introduction to Organic Chemistry*, 2nd ed., Macmillan Publishing, New York, p. 256, 1981.
(68) Grassie, N. and MacCallum, J.R., *J. Polym. Sci. Part A*, 2, 983 (1961).
(69) Fox, R.B., Isaacs, L.G., and Stokes, S., *J. Polym. Sci., Part A*, 1, 1079 (1963).
(70) Gupta, A., Liang, R., Tsay, F.D., and Moacanin, J., *Macromolecules*, 13, 1696 (1980).